Interactions between two touching spherical particles in sedimentation

Ren Sun[1] and Allen T. Chwang[2]
[1]*Department of Engineering Mechanics, Shanghai Jiao Tong University, Shanghai 200240, China*
[2]*Department of Mechanical Engineering, The University of Hong Kong, Pokfulam Road, Hong Kong, China*
(Received 29 November 2006; revised manuscript received 31 July 2007; published 31 October 2007)

A contact of a falling spherical particle with another fixed one in an unbounded viscous fluid is theoretically investigated based on a model of adding the contact interaction to the gravitational and hydrodynamic forces. The hydrodynamic interaction between the two particles is dealt with using an extended successive reflection method, with which the complete solution to the exterior velocity field around the two-particle system is constructed on the basis of the general expression given by Lamb, and then the hydrodynamic forces and torques on the two particles are obtained by integrating the fluid stress over each particle surface. The mechanical contact force is characterized by the standard friction theory with a criterion responsible for the transition from pure rolling to rolling with slip. Resorting to the dynamical equations of motion including the gravitational, hydrodynamic, and contact forces, the settling motion of a spherical particle in the vicinity of another fixed one is depicted using the fourth-order Runge-Kutta-Fehlberg method. Compared with the experimental results available in the literature, the theoretical prediction confirms two moving patterns at contact: pure rolling and rolling with slip, analyzes the dependence of the transition from one to another on the static friction coefficient and the contact separation distance between the particle surfaces, and accounts for a limitation of the quasisteady description of two interacting noncolloidal particles.

DOI: 10.1103/PhysRevE.76.046316 PACS number(s): 47.63.mf, 47.15.G−, 47.57.ef

I. INTRODUCTION

Recent investigations [1–8] have revealed that the macroscopic structure and transport properties of suspensions, such as the effective viscosity or the sedimentation velocity, depend on the hydrodynamic and contact interactions between the suspension particles. According to the Jeffrey-Onishi theory [9–11], when a smooth noncolloidal particle approaches another, the viscous fluid gives rise to a so-called lubrication force between the close particle surfaces which increasingly slows down the rate of approach, thus precluding the particle-particle contact. And, in low-Reynolds-number flows, the behavior of a moving particle would exhibit a hydrodynamic reversibility as long as the boundary conditions display the corresponding symmetry. However, experimental evidence has shown that the real particles have microscopic surface roughness elements and the particle-particle contact does occur. And such contact produces a nonhydrodynamic contact force at a minimum particle gap [6], which corresponds to the surface roughness scale on the order of 10^{-3} to 10^{-2} particle radii [12]. This contact force affects significantly the dynamical behaviors of moving particles, and leads to a symmetry breaking phenomenon. Furthermore, the bulk effect of the contact interaction makes a non-negligible contribution to the macroscopic properties of suspensions [13–18]. The categories of the contact are explored by several authors, and until now, two typical models have been proposed for the contact patterns. One is a simple stick-rotate model [3,19,20] in which both spherical particles are locked together so that the two particles translate and rotate as a rigid body. The other is a roll-slip model [3,6,8] in which one spherical particle rolls around the surface of the other with slip occurring if the maximum tangential force allowed by the mechanical friction is exceeded.

In the theoretical investigation of hydrodynamic interactions between two submerged bodies with contact at low Reynolds number, the standard friction theory has been adopted to describe the mechanical contact force [21,22], and several theoretical approaches for determining the hydrodynamic interaction between the two bodies have been developed. These include usages of reflections [23], bispherical coordinates [24,25], tangent-sphere coordinates [19], collocation methods [26], twin multipole expansions [10], asymptotic methods [27,28], and the extended successive reflections [29,30]. Although each of the methods mentioned above has individual advantages, the extended successive reflection method is of theoretical importance. The recently developed approach is an extension of reflections in which every harmonic corrective function being also a solution for the Stokes equations is established in succession to satisfy only the impenetrable boundary condition on each body surface just like images in an ideal flow [29]. And the velocity expression composed of these functions in series form is finally required to satisfy the no-slip boundary condition on each body surface. In this manner, the items in all the series expressions decay by the order $O(1/s^2)$, where s is the distance between the centers of two bodies, faster than those following from the pure reflections. This method is accurate and produces power series in iterative form of given particle radii and separation distance that are suitable for numerical computation.

The objective of this investigation is an attempt to predict combined hydrodynamic and contact interactions between two settling noncolloidal spherical particles associated with contact at low Reynolds number and describe their quasisteady behaviors by means of the extended successive reflections. To do this, the general solution for the flow field outside a particle would be expressed in harmonics and biharmonics from Lamb's representation [31] for Stokes' flow. By using two sets of transformations of harmonics and biharmonics between two coordinates [30] and the extended

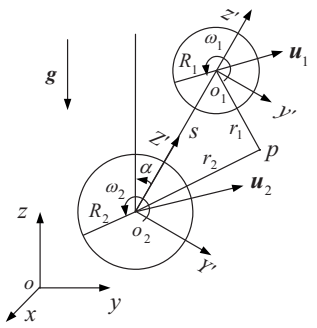

FIG. 1. Configuration of two spherical particles and the corresponding coordinates.

successive reflections, the complete solution to the velocity field around the two particles is constructed. It is then employed to predict the hydrodynamic forces and torques on these particles by integrating the fluid stress over each particle surface even as the minimum dimensionless separation ξ_m [6] between the particle surfaces is down to 10^{-4}. Dynamical equations of motion, taking account of the contact force, are adopted to describe the quasisteady motion of the two-particle system, and it may be easily solved by means of the fourth-order Runge-Kutta-Fehlberg method [32]. As an example, such a system of a particle settling around another fixed one is described. Meanwhile, the theoretical results are compared to available experimental ones in recent literature [6,8]. In comparison between the theoretical and corresponding experimental results, the limitation of the quasisteady description of two interacting noncolloidal particles is presented.

II. THEORETICAL PREDICTIONS

A. Formulation of the problem

Consider two spherical particles of radii R_1 and R_2 with densities ρ_1 and ρ_2, respectively, released in an unbounded fluid of density ρ and viscosity μ in a gravitational acceleration environment $\boldsymbol{g}$. The two particles are considered to make planar motion in the vertical y-z symmetric plane in order to simplify the analysis, as shown in Fig. 1. Particle i $(i=1,2)$, with center o_i located at $(0,y_i,z_i)$ and driven by the gravity, settles down in the fluid with a translational velocity $\boldsymbol{u}_i$ and an angular velocity ω_i with its rotation axis perpendicular to the y-z plane.

On the assumption that the fluid is incompressible and the flow due to tardy particle motion is regarded as a creeping one, the flow is described by its velocity $\boldsymbol{u}$ and hydrodynamic pressure p, satisfying the Stokes equations

$$\nabla \cdot \boldsymbol{u} = 0, \quad \nabla p - \mu \nabla^2 \boldsymbol{u} = 0, \tag{1}$$

with the no-slip boundary conditions on particle surfaces and the fluid velocity vanishing at infinity,

$$\boldsymbol{u} = \boldsymbol{u}_i + \omega_i \boldsymbol{e}_1 \times \boldsymbol{r}_i \quad \text{on } r_i = R_i \ (i = 1,2), \tag{2a}$$

$$\boldsymbol{u} \to 0 \quad \text{as } \boldsymbol{r} \to \infty, \tag{2b}$$

where $\boldsymbol{e}_{()}$ is the unit vector along the positive direction of the corresponding axis in numerical order.

B. Analytical solution for a two-particle system

Two sets of auxiliary coordinates, (x,y',z') and (x,Y',Z'), fixed at two particle centers are introduced for convenience (see Fig. 1), which can be turned into spherical ones by

$$\begin{cases} x = r_1 \sin\theta_1 \sin\varphi, \\ y' = r_1 \sin\theta_1 \cos\varphi, \\ z' = r_1 \cos\theta_1, \end{cases} \quad \text{and} \quad \begin{cases} x = r_2 \sin\theta_2 \sin\varphi, \\ Y' = r_2 \sin\theta_2 \cos\varphi, \\ Z' = r_2 \cos\theta_2. \end{cases} \tag{3}$$

From the general solution given by Lamb, the velocity field $\boldsymbol{u}$ outside an isolated spherical particle translating and rotating in a Stokes flow can be written in the (r_1,θ_1,φ) coordinates as

$$\boldsymbol{u} = \sum_{m=0}^{1} B_{3-m} \nabla \left(\frac{P_1^m \cos m\varphi}{r_1^2} \right) - \frac{A_{3-m} r_1^2}{6\mu} \nabla \left(\frac{P_1^m \cos m\varphi}{r_1^2} \right) + \frac{2A_{3-m}\boldsymbol{e}'_{3-m}}{3\mu r_1} + (-1)^{m+1} C \boldsymbol{e}'_{m+2} \left(\frac{P_1^m \cos m\varphi}{r_1^2} \right), \tag{4a}$$

and the hydrodynamic pressure due to the same flow as

$$p = \sum_{m=0}^{1} \frac{A_{3-m} P_1^m \cos m\varphi}{r_1^2} - \rho g z + p_0, \tag{4b}$$

where A, B, and C are constants to be determined by the boundary conditions, p_0 is a reference pressure, and P_1^m denotes the associated Legendre function $P_1^m(\cos\theta_1)$. Here items including A and B involve the translation of the particle and those including factor C represent its rotation.

To deal with the problem on the hydrodynamic interaction between two submerged particles in a low-Reynolds-number flow, the standard reflection method requires biharmonics as corrective functions successively to satisfy the no-slip boundary condition on each particle surface. But burdensome work in mathematical deduction makes it extremely difficult to derive a complete solution. Consequently, the extended successive reflection approach is taken into account. Such a method regards harmonics as correctors in turn to satisfy only the impenetrable conditions on each particle surface. A heuristic proof is presented here to explain why harmonics are chosen as corrective functions for boundary demands:

$$\text{If} \quad \nabla p - \mu \nabla^2 \boldsymbol{u}_0 = 0 \quad \text{and} \quad \nabla^2 \boldsymbol{u}'_{(i)} = 0 \quad (i = 1,2\ldots), \tag{5a}$$

$$\text{Then} \quad \nabla p - \mu \nabla^2 \left(\boldsymbol{u}_0 + \sum_i \boldsymbol{u}'_{(i)} \right) = 0 \quad \text{still holds}, \tag{5b}$$

where every harmonic $\boldsymbol{u}'_{(i)}$ as a corrective function satisfies only the impenetrable boundary condition on the corresponding particle surface, as depicted in Fig. 2. And the velocity

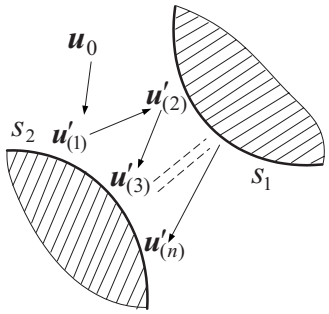

FIG. 2. Schematic description of the extended successive reflections.

field composed of these functions in series form is finally required to satisfy the no-slip boundary condition on each body surface.

In terms of expressions given by Ref. [30] with a little correction and those in the Appendix, the complete solution to the velocity field $\boldsymbol{u}$ of the ambient fluid around the two particles is constructed below:

$$\boldsymbol{u} = \sum_{i=1}^{2}\sum_{m=0}^{1} B_{i,3-m}\boldsymbol{h}'_{im} - \frac{A_{i,3-m}}{6\mu}\boldsymbol{h}''_{im} + \frac{2A_{i,3-m}\boldsymbol{h}'''_{im}}{3\mu} + (-1)^{m+1}C_i\boldsymbol{h}'''_{im}, \tag{6}$$

where boldfaces $\boldsymbol{h}'$ are elementary velocity disturbance vectors in relation to the two-particle system. One may refer to Ref. [30] for further details. Here A, B, and C are constants just like those mentioned above but for the two particles. Substituting Eq. (6) into boundary conditions (2a) leads, with manipulation, to ten algebraic equations of $A_{i,j+1}$, $B_{i,j+1}$, and C_i $(i,j=1,2)$ as

$$B_{i,3-m} = \frac{A_{i,3-m}R_i^2}{2\mu} - \frac{u'_{i,3-m}R_i^3}{2} \quad \text{for } i=1,2 \text{ and } m=0,1, \tag{7a}$$

$$B_{i,3-m}\left(\frac{1}{R_i^3} + \frac{3}{2}\sum_{k=0}^{\infty}\lambda_{i,m,1}^{(2k)}\right) + \frac{A_{i,3-m}}{\mu}\left(\frac{1}{2R_i} - \frac{1}{4}\sum_{k=0}^{\infty}\mu_{i,m,1}^{(2k)}\right) + \frac{3B_{3-i,3-m}}{2}\sum_{k=0}^{\infty}\lambda_{3-i,m,1}^{(2k+1)} - \frac{A_{3-i,3-m}}{\mu}\left(\frac{1}{4}\sum_{k=0}^{\infty}\mu_{3-i,m,1}^{(2k+1)} - (-1)^m\frac{2C_{m,1,1}R_i^2}{5}\right) = u'_{i,3-m} \quad \text{for } i=1,2 \text{ and } m=0,1, \tag{7b}$$

$$-5\left(B_{i,2}\sum_{k=0}^{\infty}\lambda_{i,1,2}^{(2k)} + B_{3-i,2}\sum_{k=0}^{\infty}\lambda_{3-i,1,2}^{(2k+1)}\right) + \frac{5}{6\mu}\left(A_{i,2}\sum_{k=0}^{\infty}\mu_{i,1,2}^{(2k)} + A_{3-i,2}\sum_{k=0}^{\infty}\mu_{3-i,1,2}^{(2k+1)}\right) + \frac{C_i}{R_i^3} + (-1)^i\frac{4A_{3-i,2}C_{1,1,2}R_i^2}{7\mu} = \omega_i \quad \text{for } i=1,2, \tag{7c}$$

where $u'_{i,j+1}$ $(i,j=1,2)$ denotes the $(j+1)$th velocity component of particle i in the (x,y',z') coordinates. Here values of $A_{i,j+1}$, $B_{i,j+1}$, and C_i $(i,j=1,2)$ are simultaneous solutions of the above ten algebraic equations.

C. Hydrodynamic forces and torques on individual particles

In order to describe a quasisteady behavior of two moving spherical particles at low Reynolds number, it is important to predict the hydrodynamic forces and torques on individual particles. The force $\boldsymbol{F}_i$ and torque T_i exerted by the fluid on particle i due to its motion and interaction with the other are given by

$$\boldsymbol{F}_i = \int_{\Sigma_i} \boldsymbol{\Pi}\cdot\boldsymbol{n}\,ds \quad \text{and} \quad T_i\boldsymbol{e}_1 = \int_{\Sigma_i} \boldsymbol{r}\times\boldsymbol{\Pi}\cdot\boldsymbol{n}\,ds \quad \text{for } i=1,2, \tag{8}$$

where Σ_i $(i=1,2)$ denotes the surface of particle i, and $\boldsymbol{n}$ is the outward normal to the surface. Here $\boldsymbol{\Pi}\cdot\boldsymbol{n}$ is the radial component of the fluid stress tensor $\boldsymbol{\Pi}$. Integrals in Eq. (8) result in, after some manipulation, the following expressions in closed form of the hydrodynamic interaction components in the (x,y',z') coordinates:

$$F'_{i,2} = \frac{4\pi R_i^3}{3}\left\{-\rho g\sin\alpha + A_{i,2}\left[\frac{-3}{R_i^3} + \frac{2}{3R_i^2}\sum_{k=0}^{\infty}(R_i^2\gamma_{i,2}^{(2k)} - 4\gamma_{i,0}^{(2k)}) + \frac{1}{2}\sum_{k=0}^{\infty}\nu_{i,1,2}^{(2k)}\right] + A_{3-i,2}\left[\frac{5C_{1,1,1}}{3} + \frac{2}{3R_i^2}\sum_{k=0}^{\infty}(R_i^2\gamma_{3-i,2}^{(2k+1)} - 4\gamma_{3-i,0}^{(2k+1)}) + \frac{1}{2}\sum_{k=0}^{\infty}\nu_{3-i,1,2}^{(2k+1)}\right] + \frac{\mu C_i}{R_i^2}\sum_{k=0}^{\infty}[4\phi_{i,0,0}^{(2k)} - R_i^2(\phi_{i,0,2}^{(2k)} + 3\phi_{i,1,2}^{(2k)})] + \frac{\mu C_{3-i}}{R_i^2}\sum_{k=0}^{\infty}\left[4\phi_{3-i,0,0}^{(2k+1)} - R_i^2(\phi_{3-i,0,2}^{(2k+1)} + 3\phi_{3-i,1,2}^{(2k+1)})\right]\right\}, \tag{9a}$$

$$F'_{i,3} = \frac{4\pi R_i^3}{3}\left\{\rho g \cos\alpha + A_{i,3}\left[\frac{-3}{R_i^3} - \frac{4}{3R_i^2}\sum_{k=0}^{\infty}(R_i^2\gamma_{i,2}^{(2k)} + 2\gamma_{i,0}^{(2k)}) + \frac{1}{3R_i^2}\sum_{k=0}^{\infty}(R_i^2\nu_{i,0,2}^{(2k)} + 2\nu_{i,0,0}^{(2k)})\right]\right.$$
$$\left. + A_{3-i,3}\left[-\frac{5C_{0,1,1}}{3} - \frac{4}{3R_i^2}\sum_{k=0}^{\infty}(R_i^2\gamma_{3-i,2}^{(2k+1)} + 2\gamma_{3-i,0}^{(2k+1)}) + \frac{1}{3R_i^2}\sum_{k=0}^{\infty}(R_i^2\nu_{3-i,0,2}^{(2k+1)} + 2\nu_{3-i,0,0}^{(2k+1)})\right]\right\}, \tag{9b}$$

$$T_i = 4\pi R_i^3\left\{-\mu C_i\left[\frac{2}{R_i^3} + \sum_{k=0}^{\infty}(\phi_{i,0,1}^{(2k)} + \phi_{i,1,1}^{(2k)})\right] - \mu C_{3-i}\sum_{k=0}^{\infty}(\phi_{3-i,0,1}^{(2k+1)} + \phi_{3-i,1,1}^{(2k+1)})\right.$$
$$\left. + \frac{2}{3}\left(A_{i,2}\sum_{k=0}^{\infty}\gamma_{i,1}^{(2k)} + A_{3-i,2}\sum_{k=0}^{\infty}\gamma_{3-i,1}^{(2k+1)}\right) + \frac{1}{6}\left(A_{i,2}\sum_{k=0}^{\infty}\nu_{i,1,1}^{(2k)} + A_{3-i,2}\sum_{k=0}^{\infty}\nu_{3-i,1,1}^{(2k+1)}\right)\right\}, \tag{9c}$$

for $i=1,2$. Here the corresponding notations are defined in a manner similar to the foregoing ones. One easily finds that letting $s\to\infty$, for these sixteen algebraic equations in (7a)–(7c) and (9a)–(9c), all coupling terms related to s vanish, and thus in the (x,y',z') coordinates

$$F'_{i,2} = -6\pi\mu R_i u'_{i,2} - \frac{4\pi}{3}\sin\alpha\rho g R_i^3, \tag{10a}$$

$$F'_{i,3} = -6\pi\mu R_i u'_{i,3} + \frac{4\pi}{3}\cos\alpha\rho g R_i^3, \tag{10b}$$

$$T_i = -8\pi\mu\omega_i R_i^3, \tag{10c}$$

for $i=1,2$. Equations (10a)–(10c) are the well-known expressions for the hydrodynamic forces and torques on two isolated quasisteadily moving spheres at a low Reynolds number in a gravitational environment. Seen from Eqs. (9a)–(9c), the tangential force expressions include such flow parameters related to the rotational effect and those with the translational effect appear also in the torque expressions as well. This implies that translation would be coupled with rotation in a two-particle system, and energy may change from a translational degree of freedom into that of a rotational one and vice versa. The phenomenon cannot be expected in a potential-flow case if the solid particles are spherical.

D. Dynamical equations of motion

This paper presents complete analytical expressions for both the exterior velocity around two spherical particles and the hydrodynamic interaction between them in a quasisteady situation without consideration of fluid inertia. Apparently, the hydrodynamic forces and torques acting on these particles are sufficient to establish dynamical equations of motion for their behaviors in low-Reynolds-number flows. If a particle-particle contact is considered in the course of two gravity-driven particles approaching each other, the dynamical equations governing their motions become

$$M_i\frac{d\boldsymbol{u}_i}{dt} = \boldsymbol{F}_i + M_i\boldsymbol{g} + \boldsymbol{f}_i, \tag{11a}$$

$$J_i\frac{d\omega_i}{dt} = T_i + \tau_i, \tag{11b}$$

for $i=1,2$. Here M_i and J_i are the mass and moment of inertia of particle i, respectively, and $\boldsymbol{f}_i$ and τ_i are the restraining force and torque exerted by the other particle, which are equal to zero except when the two particles come into contact. By virtue of these equations including the hydrodynamic interaction, gravitational force, and contact force, one may explore quasisteady behaviors of two settling particles associated with contact.

The contact interactions, $\boldsymbol{f}_i$ and τ_i $(i=1,2)$, are determined by the classical friction theory. The motion during touch is based on an *ad hoc* assumption that the contact separation distance between the particle surfaces remains approximately constant equivalent to the effective thickness of roughness elements on particle surfaces. Generally, there are two generic kinds of moving patterns during touch, pure rolling, and rolling with slip, which are characterized by the ratio of the tangential to normal forces transmitted from one surface to another [6]. For a pure rolling, the ratio is less than a critical value μ_s, the static friction coefficient, and for a rolling with slip, the ratio becomes a constant μ_k, called kinetic friction coefficient. μ_k is always smaller than μ_s.

This investigation will discuss a touch case of a particle (particle 1) moving down along the surface of another fixed one (particle 2) for simplicity. In this case, the motion during touch is described in a noninertial frame of reference. A torque and forces acting on particle 1 are shown schematically in Fig. 3. Here f_{1T} and f_{1n} are the tangential and normal components of f_1, and f_c the centrifugal force due to a circumferential motion of particle 1. Therefore the dynamical equations of motion during touch become

$$M_1R_1\dot{\omega}_1 = f_{1T} - F'_{1,2} - M_1 g\sin\alpha, \tag{12a}$$

$$J_1^*\dot{\omega}_1 = T_1 - F'_{1,2}R_1 - M_1 g\sin\alpha R_1 \tag{12b}$$

for a pure rolling, and

$$M_1\dot{u}'_{1,2} = F'_{1,2} + M_1 g\sin\alpha - \mu_k f_{1n}, \tag{12c}$$

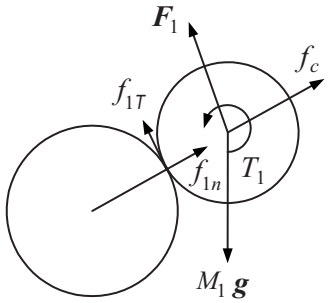

FIG. 3. Torque and forces on particle 1.

$$J_1\dot{\omega}_1 = T_1 - \mu_k f_{1n} R_1 \tag{12d}$$

for a rolling with slip. Here $J_1^* = J_1 + M_1 R_1^2$. The normal restraining force f_{1n} along the z' direction can be written as

$$f_{1n} = \frac{4}{3}\pi R_1^3(\rho_1 - \rho)g\cos\alpha - \frac{M_1 u_{1,2}'^2}{R_1 + R_2 + \xi_m R_2}. \tag{13}$$

Determination of whether sphere 1 during touch would undertake a pure rolling is based on such a criterion that

$$f_{1T} = F_{1,2}' + M_1 g \sin\alpha + M_1 R_1\left(\frac{T_1 - F_{1,2}' R_1 - M_1 g \sin\alpha R_1}{J_1'}\right) < \mu_s f_{1n} \tag{14}$$

on the premise of rolling without slip before.

III. RESULTS AND DISCUSSION

A. Comparison between theoretical results and the corresponding experimental ones

Equations (9a)–(9c), (11a), (11b), (12a)–(12d), and (13) can be employed to determine combined hydrodynamic and contact interactions between two settling noncolloidal spherical particles associated with contact at low Reynolds number, and predict a quasisteady behavior of a gravity-driven particle settling around another fixed one in an otherwise quiescent fluid. To this end, the numerical computation is the vital resort of solving these algebraic and ordinary differential equations since their analytical solutions are generally not available. The ordinary differential equations are solved using the fourth-order Runge-Kutta-Fehlberg method of integration, and the time step is adaptive according to an error tolerance of five significant figures. As each of the kth terms in the series expressions in Eqs. (9a)–(9c) behaves like $1/s^{2k}$, the truncated series in an extreme case at $k=150$ would make our numerical results accurate up to the 300th inverse power of s. And the practical calculations are carried out with an automatic increase in k until the summation of extra terms produces no significant variation within the preassigned level of accuracy even for a minimum dimensionless separation ξ_m down to 10^{-4}.

In order to compare the theoretical results with available experimental ones, let us consider a sedimentation of particle 1 with radius $R_1=0.3175$ cm and density $\rho_1=7.8$ g/cm^3 around the fixed particle 2 with radius $R_2=0.315$ cm in an unbounded viscous liquid of density $\rho=0.978$ g/cm^3 and viscosity $\mu=978$ dyn s/cm^2, subjected to a gravitational environment of $g=981$ cm/s^2. Under the balance of the buoyancy, gravity, and Stokes' drag, the terminal settling velocity of particle 1 alone, the Stokes velocity, is $u_{10}\approx 0.1533$ cm/s, and the Reynolds number therewith corresponds to $\mathrm{Re}\approx 9.7\times 10^{-5}$. The contact separation distance is set down to $\xi_m=1\times 10^{-4}$. At contact, the friction coefficient needs to be specified to match an appropriate moving pattern. The typical coefficients (cf. Ref. [6]) for well-lubricated metal-nonmetal contacts are given here $\mu_s\approx 0.15$ for a pure rolling and $\mu_k\approx 0.1$ for a rolling with slip. The whole motion during touch is determined by the contact force: as the ratio of the tangential component of the contact force to its normal one at the initial contact instant is less than a critical value μ_s, the settling particle moves in a pure rolling pattern; at the instant when the ratio exceeds the limit, the settling particle will start to roll with slip with the friction coefficient sharply decreasing to satisfy Amontons' law. The computation starts at three initial positions $z_{10}=2$ cm, $y_{10}=0.035$, 0.317, and 0.566 cm, which may evolve three typical particle-moving patterns.

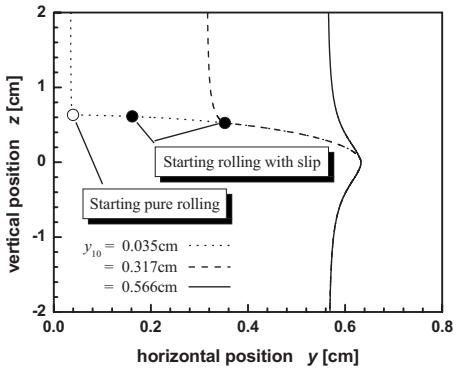

FIG. 4. Trajectories of the settling particle center around another fixed one with three initial horizontal positions.

Figure 4 shows three particle sediment trajectories. The solid line in the figure implies that particle 1 is released gently at such a critical initial horizontal position y_{10cr1} ($y_{10cr1}=0.566$ cm in the present case) that it just passes by the fixed one without touch thereafter. This trajectory exhibits a symmetry with respect to reflection in the horizontal plane $z=0$ due to the reversibility of the Stokes equations. The dashed line presents a situation in which particle 1 set free at an initial horizontal position $y_{10}=0.317$ cm would touch the fixed one and immediately roll with slip on its surface until it runs away from it. The dotted line indicates that particle 1 released motionless at an initial horizontal position $y_{10}=0.035$ cm would experience a pure rolling and subsequent rolling with slip during touch, with a sharp transition from one to another. The last two plots are asymmetric with respect to $z\rightarrow -z$. As a result, it is difficult to predict the dynamical behavior of particle 1 although the lower segments ($z<0$) of these three curves are almost overlapped. It is further deduced from the figure that if particle 1 is set free at a smaller initial horizontal position than the critical one, $y_{10}<y_{10cr1}$, then it would touch the fixed particle inevitably,

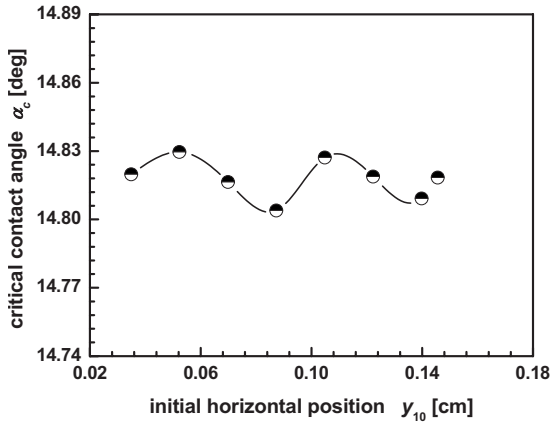

FIG. 5. The critical contact angle vs the initial horizontal position.

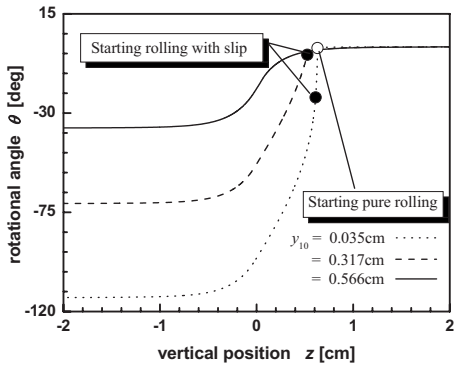

FIG. 6. Rotational angle of particle 1 vs the vertical position.

and its trajectories are asymmetric with respect to reflection in the horizontal plane $z=0$. This phenomenon obviously disobeys the prediction of reversibility of the Stokes equations. The reasonable explanation is that the contact force between the two particles during touch is responsible for the "symmetry breaking."

In addition, as presented in the figure, the numerical computation verifies the conclusion given by Ekiel-Jeżewska *et al.* [6] that there are two intervals of motion during touch: pure rolling and rolling with slip. The transition from a pure rolling to a rolling with slip is described by the critical contact angle α_c defined as a specific angle between the z' and z axes at which slip occurs. For given friction coefficients and contact separation distance, the variation of α_c with the initial horizontal position is plotted in Fig. 5. It is observed from Fig. 5 that the critical contact angle α_c is not fixed but varies in a small interval of 0.03° with the initial horizontal position. Every critical contact angle is determined by the individual initial horizontal position. The phenomenon is due to the centrifugal effect arising from the circumferential motion of particle 1 during touch. This implies that as the contact angle of the two particles is less than 14.8°, particle 1 moves in a pure rolling pattern, but as the contact angle falls into the interval between 14.83° and 90°, it takes the pattern of rolling with slip. After that, particle 1 will run away from contact. The critical value of 14.8°, equivalent to $\alpha_c = 0.258$ rad, is somewhat larger than that of the experimental data [6], $\alpha_c \leq 0.25$ rad. Such a discrepancy could originate from a little difference in μ_s and ξ_m. Furthermore, by using the try-and-error method, another critical initial horizontal position of $y_{10cr2}=0.145$ cm, equivalent to $y_{10cr2}/R_2=0.456$, is determined. When particle 1 is released at an initial horizontal position larger than y_{10cr2} but less than y_{10cr1}, it would undertake only a rolling with slip.

Figure 6 shows variation of the rotational angle θ of particle 1 against the vertical position. It is deduced from the figure that if the particle passes by the fixed one without contact, then the angular velocity plot of the moving particle exhibits symmetry with respect to $z \rightarrow -z$. This conclusion can be heuristically explained by the reversibility of the Stokes equations, i.e., $u_y(z)=-u_y(-z)$ and $u_z(z)=u_z(-z)$, and the coupling effect of the translation with rotation as well. In addition, it is seen from the figure that the initial horizontal position determines the rotational evolution of the settling particle. The smaller y_{10} is, the larger the variation of the rotational angle will be. In the contact case, the contact force not only dissipates the mechanical energy but also changes a part of the translational energy into the rotational one so that the rotational motion is no longer symmetric.

Velocity components of particle 1 against the vertical position are respectively plotted in Figs. 7 and 8 in order to compare the theoretical predictions with available experimental results in Ref. [6]. It is noted from Fig. 7 that the upper-half parts ($z>0$) of the two prediction curves in the contact cases are similar to the corresponding experimental findings with an extreme value nearly up to 4.0×10^{-2} cm/s, while their lower-half parts have smaller velocity amplitude peaks than the relevant experimental data. This is because the theoretical prediction neglects van der Waals attractions which prevent the escape of the settling particle from the surface of the fixed one, thus making it change the direction of motion. Readers can also observe from Fig. 8 that there are three major discrepancies between the theoretical predictions and the experimental results. The experimental data show that the maximum vertical velocity of the settling particle approaches 0.09 cm/s, less than its

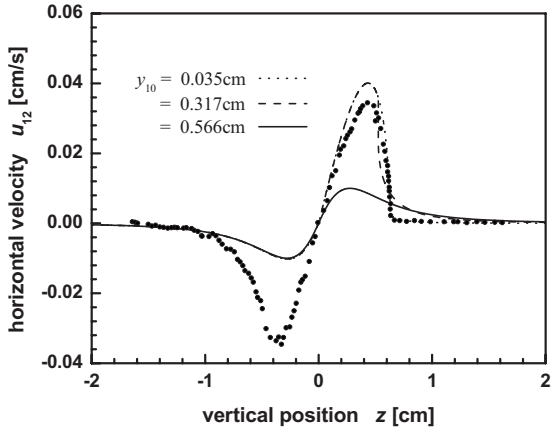

FIG. 7. Horizontal velocity of the settling particle center vs the vertical position from experiments (symbols) and theoretical predictions.

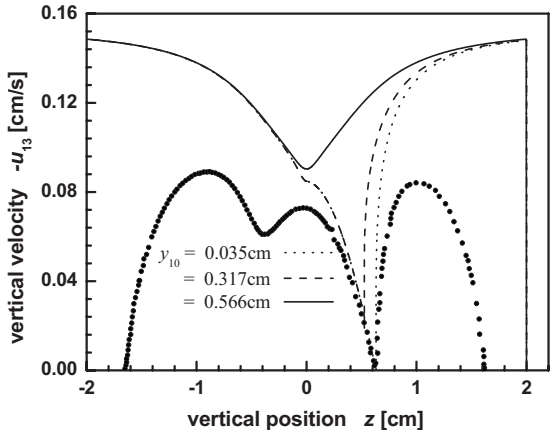

FIG. 8. Vertical velocity of the settling particle center vs the vertical position from experiments (symbols) and theoretical predictions.

Stokes velocity, and its sedimentation velocity at the final stage decreases gradually to zero instead of maintaining a constant velocity just like the theoretical prediction. These differences are mainly due to the wall effect induced by the experimental container. However, the wall effect will not be discussed in the present paper. The experimental data still show that particle 1 driven by the gravity accelerates gently up to a maximum speed after released, but the Stokes equations predict the particle almost reaches the terminal velocity at once. The reason should be that the Stokes equations do not involve the unsteady effect, and thus the Basset and added-mass forces are overlooked.

The dependences of the transition from a pure rolling to a rolling with slip on the static friction coefficient and the contact separation distance are respectively depicted in Figs. 9 and 10. The predictions are made for a given initial position, $z_{10}=2$ cm, $y_{10}=0.035$ cm. Figure 9 shows a plot of α_c vs μ_s. Note from the plot that the critical contact angle is directly proportional to the static friction coefficient. This illustrates that the typical values of $\mu_s=0.11$–0.2 for lubricated metal-nonmetal contacts do not have a nonlinear influence on the

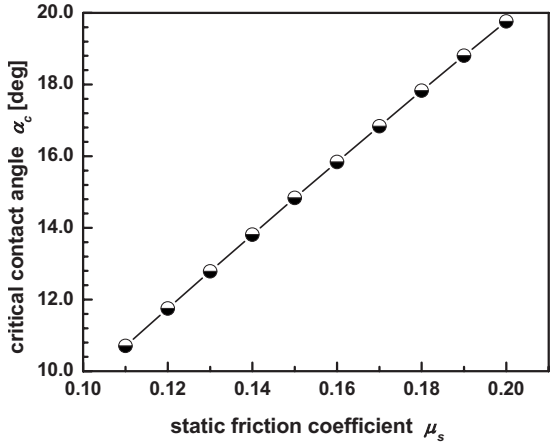

FIG. 9. Variation of the critical contact angle against the static friction coefficient with $\xi_m=1\times10^{-4}$.

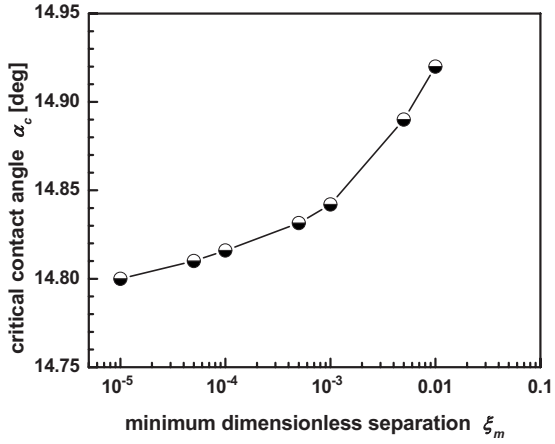

FIG. 10. Variation of the critical contact angle against the minimum dimensionless separation with $\mu_s=0.15$.

transition from a pattern to another in the present case. Figure 10 shows how the transition depends on the contact separation distance ($\xi_m=1\times10^{-5}$–1×10^{-2}). In this case, the increment of the contact gap between the particle surfaces postpones the transition. This is because an increase in the surface contact gap would decrease the ratio of f_{1T} to f_{1n}, and thus delay the translation.

B. Limitation of the quasisteady description

In order to explain the discrepancy in velocity components between the theoretical prediction and corresponding experimental result, let us discuss a quasisteady sedimentation of an isolated particle 1 at low Reynolds number, which is governed by the following dynamical equation of motion:

$$M_1\ddot{z}+6\pi\mu R_1\dot{z}+(M_1-M_d)g=0, \tag{15a}$$

with the initial conditions

$$z(0)=2 \quad \text{and} \quad \dot{z}(0)=0, \tag{15b}$$

where $M_d=4\pi\rho R_1^3/3$ is the fluid mass displaced by particle 1. Integrating Eq. (15a) with respect to time t, the vertical velocity and displacement expressions of particle 1 can be derived as

$$\dot{z}=-\frac{2(\rho_1-\rho)gR_1^2}{9\mu}\left[1-\exp\left(-\frac{9\mu t}{2\rho_1R_1^2}\right)\right], \tag{16a}$$

and

$$z=-\frac{2(\rho_1-\rho)gR_1^2}{9\mu}\left[t+\frac{2\rho_1R_1^2}{9\mu}\exp\left(-\frac{9\mu t}{2\rho_1R_1^2}\right)\right]+\frac{4(\rho_1-\rho)\rho_1gR_1^4}{81\mu^2}+2. \tag{16b}$$

By letting $t\to\infty$, Eq. (16a) gives the famous Stokes velocity. With this terminal settling velocity, particle 1 is in a dynamically balanced state, namely, the net force on the particle turns to zero. If u_{10} is chosen as a characteristic velocity, τ_0 as a time scale, R_1 as a length scale, and $\mu\, u_{10}/R_1$ is regarded

as a characteristic pressure, then the Navier-Stokes equation may be written in dimensionless form as follows:

$$\mathrm{Ns}\frac{\partial \boldsymbol{u}'}{\partial t'} + \mathrm{Re}(\boldsymbol{u}' \cdot \boldsymbol{\nabla}')\boldsymbol{u}' = -\boldsymbol{\nabla}' p' + \Delta' \boldsymbol{u}', \tag{17}$$

where Ns is the Stokes number, which is defined as $R_1^2/(\nu\tau_0)$. Here physical variables with a prime express the corresponding dimensionless ones. In the present investigation, there are two time scales for the vanishingly small Reynolds number flow. One is an interaction time τ_{01} for a particle to move a reference distance which represents an interaction range, and τ_{01} takes the form

$$\tau_{01} \sim \frac{R_1}{u_{10}} = 2.07 \text{ s}. \tag{18}$$

Another indicates a transient time τ_{02} for an isolated particle from a standstill to 99% of its terminal settling velocity, and it can be easily derived from Eq. (16a) as

$$\tau_{02} = \frac{4 \ln 10 \rho_1 R_1^2}{9\mu} = 8.227 \times 10^{-4} \text{ s}. \tag{19}$$

In the interaction situation, $\mathrm{Ns}(\tau_{01}) = 4.87 \times 10^{-5}$, so the Stokes equations may give a better approximation, but in the transition process of the settling particle, $\mathrm{Ns}(\tau_{02}) = 0.123 \sim O(1)$, the first term on the left side in Eq. (17) representing the local rate of change of the velocity is not negligible, and accordingly the unsteady Stokes equations should be employed to formulate the problem.

IV. CONCLUSIONS

Complete analytical expressions for the hydrodynamic interaction of two solid spheres at low Reynolds number in the gravitational environment are presented to describe the behavior of a noncolloidal spherical particle settling around another fixed one in a viscous fluid. The contact situation is discussed resorting to the dynamical equations of motion. They are based on a plain combination of the hydrodynamic interaction and the classical solid friction forces.

The theoretical prediction confirms two moving patterns at contact: pure rolling and rolling with slip. The three typical behaviors of a settling particle are determined by two critical initial horizontal positions. As the settling particle is released at an initial horizontal position larger than y_{10cr1} ($y_{10cr1}/R_1 = 1.78$ for given physical properties and particle sizes), it would pass by the fixed particle without touch. In the situation, its motion exhibits a symmetry with respect to $z \to -z$. As the settling particle is set free at such an initial horizontal position larger than y_{10cr2} ($y_{10cr2}/R_1 = 0.456$ in the present case) but smaller than y_{10cr1}, it would undertake only a rolling with slip. And as the settling particle is initially put in a horizontal interval, $y_{10} < y_{10cr2}$, it would experience a pure rolling and subsequent rolling with slip during touch.

Such parameters as the static friction coefficient, the contact separation distance, and the initial horizontal position would influence the transition from a pure rolling to a rolling with slip. In the present case, the typical values of the static friction coefficient for lubricated metal-nonmetal contacts have a linear influence on the transition from a pattern to another. The transition depends also on the contact separation distance, i.e., it is retarded with the increment of the contact gap between the particle surfaces. Despite given static friction coefficient and contact separation distance, the critical contact angle α_c is not fixed but varies in a small interval due to the circumferential motion of the settling particle during touch.

The process of a particle settling around another fixed particle is actually an unsteady one. Accordingly, the unsteady Stokes equations should be employed to formulate the problem. For just an interaction situation, the Stokes equations can give a better approximation, nevertheless.

ACKNOWLEDGMENTS

This research was sponsored by the National Natural Science Foundation of China under Grant No. 10372060 and by the Hong Kong Research Grants Council under Grant Number HKU 7191/03E.

APPENDIX: DERIVATION OF VELOCITY FIELDS DUE TO TWO ROTATING SPHERES

In this Appendix, the fundamental solutions to the Stokes equations for a two-rotating-sphere system will be dealt with using the extended successive reflection procedure (see Ref. [30]).

Let us first consider an initial disturbance $\boldsymbol{h}'''''_{1m,0}$ due to the rotational motion of sphere 1 is a harmonic in form, written in the (r_1, θ_1, φ) coordinates as

$$\boldsymbol{h}'''''^{[1]}_{1m,0} = \frac{P_1^m \cos m\varphi \boldsymbol{e}'_{m+2}}{r_1^2}, \quad m = 0 \text{ or } 1, \tag{A1}$$

where the superscript $[i]$ means that physical variables are expressed in the (r_i, θ_i, φ) coordinates. Here P_k^m denotes the associated Legendre function $P_k^m(\cos\theta_1)$ for convenience.

When a second sphere is released motionless in the fluid at o_2, around the sphere, $\boldsymbol{h}'''''_{1m,0}$ can be expressed by using a transformation between (r_1, θ_1, φ) and (r_2, θ_2, φ) as (cf. the Appendix in Ref. [30])

$$\boldsymbol{h}'''''^{[2]}_{1m,0} = -\boldsymbol{e}'_{m+2} \sum_{k=m}^{\infty} \phi^{(1)}_{1,m,k} r_2^k \mathrm{P}_k^m \cos m\varphi, \tag{A2}$$

where $\phi^{(1)}_{1,m,k} = (-1)^{-m} C_{m,1,k}$ and P_k^m is the associated Legendre function $P_k^m(\cos\theta_2)$. From the impenetrable boundary condition on the surface of sphere 2, a corresponding correction $\boldsymbol{h}'''''_{1m,1}$,

$$\boldsymbol{h}'''''^{[2]}_{1m,1} = \boldsymbol{e}'_{m+2} \sum_{k=m}^{\infty} \phi^{(1)}_{1,m,k} R_2^{2k+1} \frac{\mathrm{P}_k^m \cos m\varphi}{r_2^{k+1}}, \tag{A3}$$

should be put into the flow field. Based on another transformation in the same reference, $\boldsymbol{h}'''''_{1m,1}$ in the (r_1, θ_1, φ) coordinates takes the form

$$\boldsymbol{h}_{1m,1}^{\prime\prime\prime\prime[1]} = -\boldsymbol{e}'_{m+2}\sum_{k=m}^{\infty}\phi_{1,m,k}^{(2)} r_1^k P_k^m \cos m\varphi, \tag{A4}$$

where $\phi_{1,m,k}^{(2)} = (-1)^{k-m+1}\Sigma_{l=m}^{\infty} R_2^{2l+1}\phi_{1,m,l}^{(1)} C_{m,l,k}$. But the added correction makes an extra contribution to the flow field and violates the impenetrable condition on sphere 1, and then another compensating correction should be introduced to counteract the violation. Continuing the same procedure in succession leads to an infinite sequence of reflection corrections, and after some algebraic treatment, the velocity field outside the two spheres in relation to disturbance $\boldsymbol{h}_{1m,0}^{\prime\prime\prime\prime}$ finally becomes

$$\boldsymbol{h}_{1m}^{\prime\prime\prime\prime} = \boldsymbol{e}'_{m+2}\left(\frac{\mathrm{P}_1^m \cos m\varphi}{r_1^2} + \sum_{k=m}^{\infty}\frac{R_2^{2k+1}\mathrm{P}_k^m \cos m\varphi}{r_2^{k+1}}\sum_{i=0}^{\infty}\phi_{1,m,k}^{(2i+1)} + \sum_{k=m}^{\infty}\frac{R_1^{2k+1}\mathrm{P}_k^m \cos m\varphi}{r_1^{k+1}}\sum_{i=0}^{\infty}\phi_{1,m,k}^{(2i)}\right), \quad m = 0 \text{ or } 1, \tag{A5}$$

where recurrence relations of $\phi_{1,m,k}^{(i)}$ are

$$\phi_{1,m,k}^{(0)} = 0, \quad \phi_{1,m,k}^{(1)} = (-1)^{-m} C_{m,1,k},$$

$$\phi_{1,m,k}^{(2i)} = (-1)^{k-m+1}\sum_{l=m}^{\infty} R_2^{2l+1}\phi_{1,m,l}^{(2i-1)} C_{m,l,k},$$

$$\phi_{1,m,k}^{(2i+1)} = \sum_{l=m}^{\infty}(-1)^{l-m+1} R_1^{2l+1}\phi_{1,m,l}^{(2i)} C_{m,l,k}. \tag{A6}$$

Consider next the contribution to the velocity field just from initial disturbances arising from rotating sphere 2 when sphere 1 is inserted at a standstill nearby. Using the aforementioned procedure, the velocity field exterior to the whole system in relation to the initial disturbance $\boldsymbol{h}_{2m,0}^{\prime\prime\prime\prime}$, which in the (r_2, θ_2, φ) coordinates is written as

$$\boldsymbol{h}_{2m,0}^{\prime\prime\prime\prime[2]} = \frac{\mathrm{P}_1^m \cos m\varphi \boldsymbol{e}'_{m+2}}{r_2^2}, \quad m = 0 \text{ or } 1, \tag{A7}$$

is obtained below:

$$\boldsymbol{h}_{2m}^{\prime\prime\prime\prime} = \boldsymbol{e}'_{m+2}\left(\frac{\mathrm{P}_1^m \cos m\varphi}{r_2^2} + \sum_{k=m}^{\infty}\frac{R_1^{2k+1}\mathrm{P}_k^m \cos m\varphi}{r_1^{k+1}}\sum_{i=0}^{\infty}\phi_{2,m,k}^{(2i+1)} + \sum_{k=m}^{\infty}\frac{R_2^{2k+1}\mathrm{P}_k^m \cos m\varphi}{r_2^{k+1}}\sum_{i=0}^{\infty}\phi_{2,m,k}^{(2i)}\right), \quad m = 0 \text{ or } 1, \tag{A8}$$

where

$$\phi_{2,m,k}^{(0)} = 0, \quad \phi_{2,m,k}^{(1)} = (-1)^{k-m+1} C_{m,1,k},$$

$$\phi_{2,m,k}^{(2i)} = \sum_{l=m}^{\infty}(-1)^{l-m+1} R_1^{2l+1}\phi_{2,m,l}^{(2i-1)} C_{m,l,k},$$

$$\phi_{2,m,k}^{(2i+1)} = (-1)^{k-m+1}\sum_{l=m}^{\infty} R_2^{2l+1}\phi_{2,m,l}^{(2i)} C_{m,l,k}. \tag{A9}$$

[1] P. A. Arp and S. G. Mason, J. Colloid Interface Sci. **61**, 21 (1977); **61**, 44 (1977).
[2] F. Parsi and F. Gadala-Maria, J. Rheol. **32**, 725 (1987).
[3] R. H. Davis, Phys. Fluids A **4**, 2607 (1992).
[4] S. Zeng, E. T. Kerns, and R. H. Davis, Phys. Fluids **8**, 1389 (1996).
[5] M. P. Petrich and D. L. Koch, Phys. Fluids **10**, 2111 (1998).
[6] M. L. Ekiel-Jeżewska, F. Feuillebois, N. Lecoq, K. Masmoudi, R. Anthore, F. Bostel, and E. Wajnryb, Phys. Rev. E **59**, 3182 (1999).
[7] K. P. Galvin, Y. Zhao, and R. H. Davis, Phys. Fluids **13**, 3108 (2001).
[8] M. L. Ekiel-Jeżewska, N. Lecoq, R. Anthore, F. Bostel, and F. Feuillebois, Phys. Rev. E **66**, 051504 (2002).
[9] D. J. Jeffrey and Y. Onishi, ZAMP **35**, 634 (1984).
[10] D. J. Jeffrey and Y. Onishi, J. Fluid Mech. **139**, 261 (1984).
[11] S. Kim and S. J. Karrilla, *Microhydrodynamics: Principles and Selected Applications* (Butterworth-Heinemann, Boston, 1991).
[12] J. R. Smart and D. T. Leighton, Jr., Phys. Fluids A **1**, 52 (1989).
[13] R. H. Davis and N. A. Hill, J. Fluid Mech. **236**, 513 (1992).
[14] R. H. Davis, J. Fluid Mech. **310**, 325 (1996).
[15] F. R. da Cunha and E. J. Hinch, J. Fluid Mech. **309**, 211 (1996).
[16] B. Cichoki, M. L. Ekiel-Jeżewska, and E. Wajnryb, J. Chem. Phys. **111**, 3265 (1999).
[17] H. J. Wilson and R. H. Davis, J. Fluid Mech. **421**, 339 (2000).
[18] B. Cichoki, M. L. Ekiel-Jeżewska, P. Szymczak, and E. Wajnryb, J. Chem. Phys. **117**, 1231 (2002).
[19] A. Nir and A. Acrivos, J. Fluid Mech. **59**, 209 (1973).
[20] M. Tabatabaian and R. G. Cox, Int. J. Multiphase Flow **17**, 395 (1991).
[21] F. P. Bowden and D. Tabor, *The Friction and Lubrication of Solids* (Clarendon, Oxford, 1950).
[22] K. L. Johnson, *Contact Mechanics* (Cambridge University Press, Cambridge, England, 1985).
[23] J. Happel and H. Brenner, *Low Reynolds Number Hydrodynamics* (Noordhoff, Leiden, 1991).
[24] M. Stimson and G. B. Jeffery, Proc. R. Soc. London, Ser. A **111**, 110 (1926).
[25] M. E. O'Neill and S. R. Majumdar, Z. Angew. Math. Phys. **21**, 164 (1970).
[26] P. Ganatos, R. Pfeffer, and S. Weinbaum, J. Fluid Mech. **84**, 79 (1978).
[27] M. E. O'Neill and K. Stewartson, J. Fluid Mech. **27**, 705

(1967).
[28] D. J. Jeffrey, Mathematika **29**, 58 (1982).
[29] R. Sun and A. T. Chwang, Theor. Comput. Fluid Dyn. **15**, 11 (2001).
[30] R. Sun and W. R. Hu, Phys. Fluids **15**, 3015 (2003).
[31] H. Lamb, *Hydrodynamics* (Cambridge University Press, Cambridge, England, 1932).
[32] W. Cheney and D. Kincaid, *Numerical Mathematics and Computing* (Brooks/Cole, Pacific Grove, CA, 1999).